An EQT-based cDFT approach for thermodynamic properties of confined fluid mixtures

M. H. Motevaselian and N. R. Aluru[a)]
Department of Mechanical Science and Engineering, Beckman Institute for Advanced Science and Technology, University of Illinois at Urbana-Champaign, Urbana, Illinois 61801, USA

(Received 24 January 2017; accepted 27 March 2017; published online 17 April 2017)

We present an empirical potential-based quasi-continuum theory (EQT) to predict the structure and thermodynamic properties of confined fluid mixtures. The central idea in the EQT is to construct potential energies that integrate important atomistic details into a continuum-based model such as the Nernst-Planck equation. The EQT potentials can be also used to construct the excess free energy functional, which is required for the grand potential in the classical density functional theory (cDFT). In this work, we use the EQT-based grand potential to predict various thermodynamic properties of a confined binary mixture of hydrogen and methane molecules inside graphene slit channels of different widths. We show that the EQT-cDFT predictions for the structure, surface tension, solvation force, and local pressure tensor profiles are in good agreement with the molecular dynamics simulations. Moreover, we study the effect of different bulk compositions and channel widths on the thermodynamic properties. Our results reveal that the composition of methane in the mixture can significantly affect the ordering of molecules and thermodynamic properties under confinement. In addition, we find that graphene is selective to methane molecules. *Published by AIP Publishing.* [http://dx.doi.org/10.1063/1.4979896]

I. INTRODUCTION

The physics and properties of confined fluids and their mixtures in nano- to micro-size pores are quite different than those in the macroscopic scale (bulk).[1–3] The major reason for this is the inhomogeneity imposed by the confined environment. The interplay between the wall-fluid and the fluid-fluid interactions significantly alters the molecular configuration, structural correlations, and thermodynamic and dynamical properties of a confined fluid in comparison to its bulk phase. As a corollary, this leads to the observation of unusually high pressure,[4,5] existence of different phases,[6,7] dynamical anomalies,[8,9] wetting and capillary phenomena[10] for fluids confined in narrow pores ranging from few Angstroms to micrometers. Confined fluids have many applications such as nanofiltration,[11–14] drug delivery,[15,16] enhanced oil recovery,[17,18] nano-super-compressors,[19] lubrication,[20] and geophysical applications.[21] Thus, to be able to design a novel nanofluidic device, the foremost step is to study and understand the physics of the confined fluid and obtain atomic-level insights into their unusual properties. To explain the molecular origin of the various phenomena occurring in the confinement, in addition to the experiments, both theory and computer simulations are of critical importance. Moreover, in some cases obtaining a molecular insight from experiments may not be accessible; thus, theory and computer simulations become viable tools to understand the underlying physics.

Molecular simulation techniques, such as molecular dynamics (MD) and Monte Carlo (MC) simulations, have been extensively used to study the thermodynamic and dynamical properties of confined fluids at the atomic level.[22–24] However, these techniques can be computationally expensive to study systems of multiple time and length scales. On the other hand, although classical continuum theories, such as Navier-Stokes equations, are computationally efficient, they fail to accurately predict the properties of the atomically confined systems.[25] Therefore, there is a need to develop a multiscale method that is as fast as classical continuum methods, and as accurate as atomistic simulations.

An empirical potential-based quasi-continuum theory (EQT) is a multiscale approach that provides a framework to seamlessly integrate atomistic details into a continuum-based model such as the Nernst-Planck equation. The main idea in EQT is to calculate the potential energies in a continuum approximation that involves information developed at the molecular level. EQT was first studied to predict the structure and potential of mean force (PMF) profiles of Lennard-Jones (LJ) fluids in slit-like channels ranging from few Angstroms to hundreds of nano-meters width.[26,27] Later, it was extended to more complex molecules such as carbon dioxide and water with electrostatic interactions.[28–30] In these studies, the effect of anisotropic electrostatic forces is taken into account by using the coarse-grained (CG) potentials from the detailed all-atom level. EQT is a robust and fast approach for providing accurate density and PMF profiles for confined fluids. Recently, it has been shown that EQT can be combined with the classical density functional theory (cDFT), i.e., EQT-cDFT, to predict the structure of binary mixtures[31] and thermodynamic properties of single component Lennard-Jones fluids.[32]

cDFT is a theoretical framework rooted in the statistical mechanics, well-suited for studying the properties of

a)aluru@illinois.edu

inhomogeneous fluids under the influence of an arbitrary external potential. It is based on the theorem that the free energy functional of the fluid is universal and independent of the external potential responsible for the inhomogeneity.[10,33–36] However, the theorem does not give the exact functional form; thus, many efforts have been devoted to provide an approximate functional form for the excess Helmholtz free energy. Due to its simplicity and convenience, mean field theory (MFT) is widely used in many of the cDFT theories. However, there are both quantitative and even qualitative discrepancies reported between MFT and molecular simulation results.[37,38] There exist more sophisticated treatments based on weighted-density approximation (WDA)[39–41] or more specifically fundamental measure theory (FMT),[42,43] perturbative methods,[44–46] and the coarse-grained lattice gas model.[47] Other methods and recent developments of the cDFT are contained in Ref. 48.

In this work, we use the EQT potentials to construct the excess Helmholtz free energy and use the EQT-based cDFT grand potential to obtain various thermodynamic properties of the confined fluid mixtures. We demonstrate the EQT-cDFT method by studying the binary mixture of methane and hydrogen molecules confined in graphene nano-slit channels. The remainder of the paper is organized as follows. In Sec. II, we describe the theory of the EQT-cDFT approach for mixtures and methods to compute the thermodynamic properties, such as local pressure tensor, surface tension, and solvation force. In Sec. III, we provide the details of simulation for both EQT-cDFT and MD simulations. In Sec. IV, we present the results for the binary mixture of methane and hydrogen molecules confined in graphene slit pores in equilibrium with two different bulk molar compositions. Finally, we draw conclusions in Sec. V.

II. THEORY AND METHODS

In general, for a confined fluid mixture, the total potential per particle at a given location $\mathbf{r}$ is the sum of the wall-fluid and the fluid-fluid potentials. In EQT, the wall-fluid potential of the ith component is expressed as

$$U_i^{\mathrm{wf}}(\mathbf{r}) = \int \rho_{\mathrm{w}}(\mathbf{r}')u_i^{\mathrm{wf}}(r)d\mathbf{r}', \tag{1}$$

where $r = |\mathbf{r}-\mathbf{r}'|$, wall atoms are kept fixed and represented by a single density distribution ρ_{w}, and $u_i^{\mathrm{wf}}(r)$ is the effective pair potential between the ith fluid component and the wall atom. Unlike the wall-fluid potential, a complete description of an inhomogeneous fluid requires the knowledge of density and pair correlation function, $g^{(2)}(\mathbf{r},\mathbf{r}')$, that contains the information of particle-particle spatial correlations between the points $\mathbf{r}$ and $\mathbf{r}'$. Thus, the fluid-fluid potential can be expressed as

$$U_i^{\mathrm{ff}}(\mathbf{r}) = \sum_{j=1}^{m}\int \rho(\mathbf{r}')u_{ij}^{\mathrm{ff}}(r)g_{ij}^{(2)}(\mathbf{r},\mathbf{r}')d\mathbf{r}', \tag{2}$$

where m is the number of fluid species in the mixture and $u_{ij}^{\mathrm{ff}}(r)$ is the effective pair potential between components i and j. The challenging term in Eq. (2) is the pair correlation function, as its inhomogeneity makes the calculations intractable.[49] Thus, in order to proceed further, we need to make an approximation for the pair correlation function. Among different approximations, MFT has been widely used in the cDFT literature to treat long-range attractions in the excess part of the intrinsic Helmholtz free energy.[33,50,51] In MFT, the structural correlations are neglected and thus, $g^{(2)}(\mathbf{r},\mathbf{r}')$ is approximated by 1. Despite its convenience, MFT can be quantitatively problematic and even sometimes qualitatively incorrect.[37,38] To circumvent these problems, there are approaches that approximate the inhomogeneous pair distribution function by the bulk radial distribution function (RDF), $g(r)$.[52–54] There is also a recent study, which approximates the pair distribution function of the inhomogeneous hard sphere fluids.[55] The approximated function has been successfully tested at a hard wall and near a single fixed hard sphere. In this study, the pair distribution function is approximated by the RDF of uniform hard spheres at the bulk density, ρ_b, i.e.,

$$g^{(2)}(\mathbf{r},\mathbf{r}') \approx g^{hs}(r). \tag{3}$$

The RDFs are obtained using existing analytical expressions for additive hard sphere mixtures based on Percus-Yevick approximation,[56,57] and the hard sphere diameters are calculated by the Barker and Henderson's relation.[58] However, the hard sphere RDF approximation may not accurately reproduce the properties of a real fluid and can be problematic for inhomogenous systems.[55] Therefore, to account for these shortcomings, we add a correlation-correction potential, $u_{\mathrm{ccp}}^{\mathrm{ff}}$, and reformulate Eq. (2) as

$$U_i^{\mathrm{ff}}(\mathbf{r}) = \sum_{j=1}^{m}\int \rho(\mathbf{r}')\left(u_{ij}^{\mathrm{ff}}(r)g_{ij}^{\mathrm{hs}}(r) + u_{\mathrm{ccp},ij}^{\mathrm{ff}}(r)\right)d\mathbf{r}'. \tag{4}$$

In EQT, $u_{\mathrm{ccp}}^{\mathrm{ff}}$ is modeled using uniform cubic B-splines as

$$u_{\mathrm{ccp}}^{\mathrm{ff}}(r) = \begin{bmatrix}1 & t & t^2 & t^3\end{bmatrix}\frac{1}{6}\begin{bmatrix}1 & 4 & 1 & 0\\ -3 & 0 & 3 & 0\\ 3 & -6 & 3 & 0\\ -1 & 3 & -3 & 1\end{bmatrix}\begin{bmatrix}c_j\\ c_{j+1}\\ c_{j+2}\\ c_{j+3}\end{bmatrix}, \tag{5}$$

where the separation interval from 0 to the cutoff, $R_{\mathrm{cut}}^{\mathrm{ff}}$, is discretized into $n-1$ segments, $\{r_0, r_1, r_2, \ldots, r_{n-1}\}$, of equal size $\Delta r = R_{\mathrm{cut}}^{\mathrm{ff}}/(n-1)$ such that $r_i = i\times\Delta r$ $(i \in (0\ldots n-1))$, $\{c_0, c_1, c_2, \ldots, c_{n+1}\}$ are the spline knots, the index j satisfies the condition $r_j \le r < r_{j+1}$, and $t = \frac{r-r_j}{\Delta r}$.

To study the thermodynamics of the confined fluid system that is in equilibrium with a bulk reservoir, the relevant thermodynamic potential is the grand potential, Ω. For a fluid mixture confined between two flat surfaces of area A, the change in grand potential caused by an infinitesimal change of thermodynamic state is given by

$$\mathrm{d}\Omega = -S\mathrm{d}T - P\mathrm{d}V - \sum_{i=1}^{m}N_i\mathrm{d}\mu_i + 2\gamma\mathrm{d}A - f_{\mathrm{S}}A\mathrm{d}H, \tag{6}$$

where S is the entropy, T is the temperature, P is the pressure, V is the volume, N_i is the number of the fluid particles of component i, μ_i is the chemical potential of the fluid particles of component i, γ is the wall-fluid surface tension, H is the channel width, and f_{S} is the solvation force. Knowing the grand potential, we can obtain any thermodynamic property by taking the appropriate derivatives of Ω according to Eq. (6). For this purpose, we use the classical density functional theory (cDFT), which gives an expression for the grand potential as a

function of the confined fluid density. Thus, Ω can be written as

$$\Omega\left[\{\rho_i(\mathbf{r})\}\right] = F\left[\{\rho_i(\mathbf{r})\}\right] + \sum_{i=1}^{m}\int\left(V_i^{\text{ext}}(\mathbf{r}) - \mu_i\right)\rho_i(\mathbf{r})d\mathbf{r}, \tag{7}$$

where F denotes the intrinsic Helmholtz free energy and V_i^{ext} is the external potential acting on the fluid component i. The Helmholtz free energy has contributions from the ideal and excess part

$$F\left[\{\rho_i(\mathbf{r})\}\right] = F^{\text{id}}\left[\{\rho_i(\mathbf{r})\}\right] + F^{\text{ex}}\left[\{\rho_i(\mathbf{r})\}\right], \tag{8}$$

where the ideal part is exactly known, and it is given by

$$F^{\text{id}}\left[\{\rho_i(\mathbf{r})\}\right] = k_{\text{B}}T\sum_{i=1}^{m}\int\rho_i(\mathbf{r})\left(\ln\left(\rho_i(\mathbf{r})\Lambda_i^3\right) - 1\right)d\mathbf{r}, \tag{9}$$

where k_{B} is the Boltzmann constant, $\Lambda_i = \left(\frac{2\pi\hbar^2}{m_i k_{\text{B}}T}\right)^{\frac{1}{2}}$ is the thermal de-Broglie wavelength, $\hbar$ is reduced Planck's constant, and m_i is the mass of the ith atom. Unlike the ideal part, the excess part of the Helmholtz free energy accounts for non-ideality due to the existing inter-molecular interactions. The treatment of this part is rather intractable, since it contains the information about correlations between the particles.[10,59,60] There are approaches that provide functional forms for F^{ex} based on the fundamental-measure theory (FMT),[61,62] modified FMT (MFMT),[63,64] first-order mean-spherical approximation (FMSA),[65] accurate empirical equation of state,[41] and statistical associating fluid theory (SAFT).[54,66–69] In this study, similar to our previous work,[31,32] we use the EQT fluid-fluid potential (Eq. (2)) to construct the excess part of the Helmholtz free energy,

$$F^{\text{ex,EQT}}\left[\{\rho_i(\mathbf{r})\}\right] = \frac{1}{2}\sum_{i=1}^{m}\int\rho_i(\mathbf{r}')U_i^{\text{ff}}(\mathbf{r}')d\mathbf{r}'. \tag{10}$$

Due to the chemical equilibrium condition between a confined fluid system and a bulk reservoir, the chemical potential of each fluid component in Eq. (7) is same as fluid components of the homogeneous phase, i.e., $\mu_i = \mu_{i,\text{b}}$. Furthermore, we can split the bulk chemical potential into the ideal and the excess part, i.e.,

$$\mu_{i,\text{b}} = \mu_{i,\text{b}}^{\text{id}} + \mu_{i,\text{b}}^{\text{ex}}, \tag{11}$$

where the ideal part can be written as

$$\mu_{i,\text{b}}^{\text{id}} = k_{\text{B}}T\ln\left(\rho_{i,\text{b}}\Lambda_i^3\right). \tag{12}$$

From the definition of the chemical potential, $\mu_{i,\text{b}}^{\text{ex}} = \left(\frac{\partial F_{\text{b}}^{\text{ex}}}{\partial\rho_{i,\text{b}}}\right)_T$, and applying Eq. (10) in the bulk phase, it is easy to show that the excess part of the bulk chemical potential is equal to the EQT bulk fluid-fluid potential, U_{b}, i.e.,

$$\mu_{i,\text{b}}^{\text{ex}} = U_{i,\text{b}}, \tag{13}$$

where $U_{i,\text{b}}$ is obtained by applying Eq. (4) in the bulk phase,

$$U_{i,\text{b}} = 4\pi\sum_{j=1}^{m}\rho_{j,\text{b}}\int_0^{R_{\text{cut}}^{\text{ff}}} r^2\left(u_{ij}^{\text{ff}}(r)g_{ij}^{\text{hs}}(r) + u_{\text{ccp},ij}^{\text{ff}}(r)\right)dr. \tag{14}$$

In this study, the external potential acting on the fluid mixture is only the wall-fluid interaction, i.e., $V_i^{\text{ext}}(\mathbf{r}) = U_i^{\text{wf}}(\mathbf{r})$. Hence, using Eqs. (7)–(13), the grand potential in the EQT-cDFT formalism can be written as

$$\begin{aligned}\Omega^{\text{EQT}}\left[\{\rho_i(\mathbf{r})\}\right] = \sum_{i=1}^{m}\Bigg(&k_{\text{B}}T\int\rho_i(\mathbf{r})\left[\ln\frac{\rho_i(\mathbf{r})}{\rho_{i,\text{b}}} - 1\right]d\mathbf{r}\\ &+\frac{1}{2}\int\rho_i(\mathbf{r})U_i^{\text{ff}}(\mathbf{r})d\mathbf{r}\\ &+\int\rho_i(\mathbf{r})\left(U_i^{\text{wf}}(\mathbf{r}) - U_{i,\text{b}}\right)d\mathbf{r}\Bigg).\end{aligned} \tag{15}$$

At equilibrium, the grand potential is minimum with respect to the density distributions; thus, from the variational principle given as

$$\left.\frac{\partial\Omega^{\text{EQT}}\left[\{\rho_i(\mathbf{r})\}\right]}{\partial\rho_i}\right|_{eq} = 0, \tag{16}$$

the equilibrium density profile of each species satisfies

$$\rho_i(\mathbf{r}) = \rho_{i,\text{b}}\exp\left(-\frac{1}{k_{\text{B}}T}\left(U_i^{\text{ff}}(\mathbf{r}) + U_i^{\text{wf}}(\mathbf{r}) - U_{i,\text{b}}\right)\right). \tag{17}$$

Using an iterative method such as Picard iteration, Eqs. (17), (2), and (1) can be solved self-consistently to obtain the equilibrium density profiles of the confined fluid mixture.

The inhomogenous fluid mixture we consider in this study is confined in slit pores made up of two graphene sheets infinitely long in the xy plane, located at $z = 0$ and $z = H$. Due to the planar geometry, we will assume that all the mean quantities vary only in the z direction. In this work, we compute thermodynamic quantities such as average densities, local pressure tensor, surface tension, and solvation force for different bulk mixture compositions.

Studying the local pressure tensor profiles in an inhomogenous fluid system is important from both the industrial and scientific point of view. For homogeneous fluids, the pressure tensor is isotropic (i.e., $P_{\text{xx}} = P_{\text{yy}} = P_{\text{zz}}$), whereas in a confined fluid, it is anisotropic and varies spatially. For slit channels, due to the symmetry in the lateral dimensions, the off-diagonal terms in the local pressure tensor are zero, and the relevant quantities are the normal, $P_{\text{n}}(z)$, and lateral, $P_l(z)$, pressure profiles. Moreover, the condition of mechanical equilibrium requires that the normal pressure be constant across the channel[70] and be equal to the average force per unit area exerted by the fluid molecules on the wall.

To obtain P_{n}, one can use the central difference method to calculate the derivative of the grand potential with respect to the channel width.[32] This method is also analogous to the volume perturbation expressions proposed by de Miguel and Jackson[71] in the context of vapour-liquid interfaces. Alternatively, from the balance of the forces in the confined direction, the normal pressure can be calculated based on the average density and the wall-fluid potential,[72] i.e.,

$$P_{\text{n}}(H) = -\sum_{i=1}^{m}\int_0^H\left(\rho_i(z)\frac{dU_i^{\text{wf}}(z)}{dz}\right)dz. \tag{18}$$

Unlike the normal pressure, the lateral pressure is not constant across the channel and varies in the z direction. For a planar system, it is possible to define the lateral pressure as

the negative of the grand potential density, $\omega(z)$;[73–75] thus from Eq. (15), P_l can be calculated as

$$P_l(z) = -\sum_{i=1}^{m}\left(k_B T \rho_i(z)\left[\ln\frac{\rho_i(z)}{\rho_{i,b}} - 1\right] + \frac{1}{2}\rho_i(z)U_i^{ff}(z) + \rho_i(z)\left(U_i^{wf}(z) - U_{i,b}\right)\right). \quad (19)$$

We can further simplify Eq. (19), by substituting the density profile from Eq. (17) and reformulate the lateral pressure in the EQT-cDFT framework as

$$P_l(z) = \sum_{i=1}^{m}\left(k_B T \rho_i(z) + \frac{1}{2}\rho_i(z)U_i^{ff}(z)\right). \quad (20)$$

The surface tension, γ, can be calculated using the thermodynamic or the mechanical route. The thermodynamic definition is based on the amount of isothermal work required to increase the interface by unit area, i.e., $\gamma = \frac{1}{2}\left(\frac{\partial\Omega}{\partial A}\right)_{T,\mu,L}$ for a slit-channel system. According to the mechanical definition, for planar systems, the surface tension can be calculated based on the integral difference of the tangential and normal components of the pressure tensor profiles along the confined direction,[73,76] i.e.,

$$\gamma(H) = \frac{1}{2}\int_0^H (P_n - P_l(z))\,dz. \quad (21)$$

Finally, the quantity f_S, which is commonly referred to as solvation force, is actually the average force per unit area exerted by the fluid molecules normal to the surface.[77] Hence, the solvation force has a unit of pressure and can be calculated as

$$f_S(H) = P_n(H) - P_b, \quad (22)$$

where P_b is the fluid mixture bulk pressure.

III. SIMULATION DETAILS

To demonstrate the EQT-cDFT approach, we consider a binary mixture of methane and hydrogen molecules confined in graphene slit channels with varying bulk compositions (see Fig. 1). The bulk compositions considered in this study are 30:70 and 70:30 CH_4/H_2—the first is a hydrogen-rich bulk reservoir ($x_m = 0.3$) and the second is a methane-rich mixture ($x_m = 0.7$) with a total bulk density of 17.73 atoms/nm^3. Methane and hydrogen molecules along with graphene carbon atoms are modelled as spherical Lennard-Jones particles, interacting via standard 12-6 LJ potential,

$$u(r) = \frac{C_{12}}{r^{12}} - \frac{C_6}{r^6}, \quad (23)$$

where C_{12} and C_6 are the usual LJ parameters to be specified for each interaction. Table I summarizes the LJ parameters used in the MD simulations.[78] MD simulations are performed in the canonical ensemble (NVT) using the GROMACS[79] software. A cutoff of 1.524 nm(=$4\sigma_m$, where σ_m is the length-scale parameter for LJ interaction between methane molecules) is used for all the interactions. To maintain the temperature at 300 K, Nosé-Hoover thermostat is used with a time constant of 0.2 ps. All systems are equilibrated for 2 ns, following a production run of 8 ns with 1 fs time step.

TABLE I. LJ interaction parameters for methane (CH4) and hydrogen (H2) molecules and graphene carbon (C) atom pairs.

	C_{12} (kJ/mol)	C_6 (kJ/mol)	σ (nm)
C–C	$0.222\,22 \times 10^{-5}$	$0.143\,85 \times 10^{-2}$	0.340 00
C–H2	$0.106\,52 \times 10^{-5}$	$0.107\,49 \times 10^{-2}$	0.315 75
C–CH4	$0.103\,18 \times 10^{-4}$	$0.470\,09 \times 10^{-2}$	0.360 50
H2–H2	$0.475\,63 \times 10^{-6}$	$0.775\,25 \times 10^{-3}$	0.291 50
H2–CH4	$0.521\,17 \times 10^{-5}$	$0.360\,58 \times 10^{-2}$	0.336 25
CH4–CH4	$0.460\,85 \times 10^{-4}$	$0.150\,66 \times 10^{-1}$	0.381 00

Nano-channels considered in this study consist of two graphene layers extended in the x–y plane and separated by a distance H in the z-direction. The lateral dimensions of the sheets are 3.834 × 3.689 nm^2, and the channel width is varied from $2\sigma_m$ to $15\sigma_m$ with an increment of $0.25\sigma_m$. The periodic boundary condition is applied in all the directions with an extra vacuum of $20\sigma_m$ in the z direction (perpendicular to the graphene layers) to avoid slab-slab interactions between periodic images. During the simulation, carbon atoms are kept frozen, i.e., their positions are not updated; thus, thermal vibrations of graphene layers are suppressed.

The average density of each species inside the channel can be obtained from the EQT-cDFT approach,[31]

$$\rho_{i,avg} = \frac{N_i}{A \times H}, \quad (24)$$

where N_i is the number of molecules of component i and A is the area of the graphene sheet. The average densities for methane and hydrogen molecules in various size channels are given in Table II. To calculate the MD local stress tensor, we use the GROMACS-LS code by Vanegas *et al.*,[80] which is based on the Hardy-Mudroch procedure. As mentioned in Sec. II, due to the mechanical equilibrium, P_n is constant across the nanopore. Therefore, for a large enough channel (e.g., $15\sigma_m$) with a well-formed bulk region in the middle, P_n should be equal to the mixture bulk pressure. We use this fact to verify the GROMACS-LS code for our simulation purposes. We observe that the normal pressure obtained from the code is constant along the z direction, and it is equal to the mixture normal pressure calculated from the total force perpendicular to the

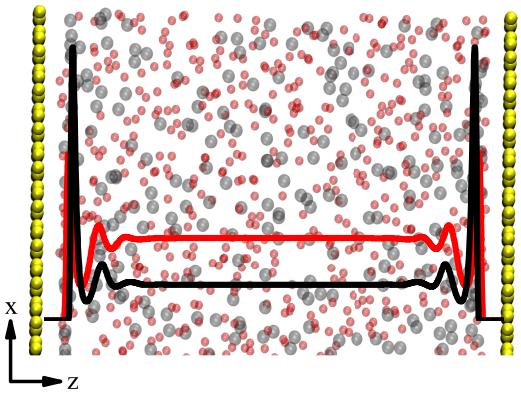

FIG. 1. Schematic representation of a binary mixture of methane (black) and hydrogen (red) molecules confined between two graphene sheets (yellow).

TABLE II. Average fluid densities (nm^{-3}) in MD simulations of various size channels for different bulk molar compositions.

ρ_{avg}	$15\sigma_m$	$10\sigma_m$	$9\sigma_m$	$8\sigma_m$	$7\sigma_m$	$6\sigma_m$	$5\sigma_m$	$4\sigma_m$	$3\sigma_m$	$2\sigma_m$
H2(x_m = 0.3)	11.02	10.33	10.10	9.81	9.46	8.97	8.27	7.24	5.38	2.23
H2(x_m = 0.7)	4.72	4.42	4.33	4.20	4.03	3.83	3.52	3.01	2.10	0.74
CH4(x_m = 0.3)	5.60	5.75	5.79	5.84	5.94	6.03	6.16	6.35	6.68	6.96
CH4(x_m = 0.7)	11.86	11.60	11.50	11.39	11.24	11.04	10.76	10.34	9.65	8.07

wall,[81]

$$P_n = \frac{|\sum_{i=1}^{N_f} F_{z,i}^{wf}|}{A}, \tag{25}$$

where N_f is the total number of fluid molecules (hydrogen and methane) and $F_{z,i}^{wf}$ is the z component of the force produced by molecule i on the wall. Other thermodynamic properties such as surface tension and solvation force can be calculated from Eqs. (21) and (22) using the values in the local pressure tensor.

Similar to the MD simulations, in the EQT-cDFT approach, we use the 12-6 Lennard-Jones potential to describe the pair interactions between different LJ particles. The same interaction parameters (see Table I) as in MD simulations are used in our quasi-continuum framework. The correlation-correction potentials are modeled using cubic B-splines, which provide a numerically robust way of obtaining accurate density profiles along with other thermodynamic properties. Potential of mean force (PMF) matching technique[30] is employed to optimize structurally consistent spline knot values. The knot values for different fluid-fluid interactions are optimized based on the $15\sigma_m$ channel, which is large enough so that the layered structure and bulk region are well formed for both hydrogen and methane. In the PMF matching technique for mixtures, the mean square error in each fluid component density profile is minimized such that the target potential energy is reproduced to the desired tolerance. Hence, to an arbitrary constant, the resulting PMFs can be used to reproduce density profiles. Thus, to correctly capture the lateral pressure profiles, the methane and hydrogen total PMF profiles are shifted by 1.33 and 16.32 kJ/mol for $x_m = 0.3$ and by −13.66 and 25.35 kJ/mol for $x_m = 0.7$, respectively. More details on the optimization procedure and PMF matching technique can be found in Ref. 30.

IV. RESULTS AND DISCUSSION

Fig. 2 shows the density profiles of methane and hydrogen molecules inside the slit graphene channels in equilibrium with hydrogen and methane-rich bulk mixtures. The equilibrium density profiles from the EQT-cDFT agree well with the MD simulations for various channel widths. Both methane

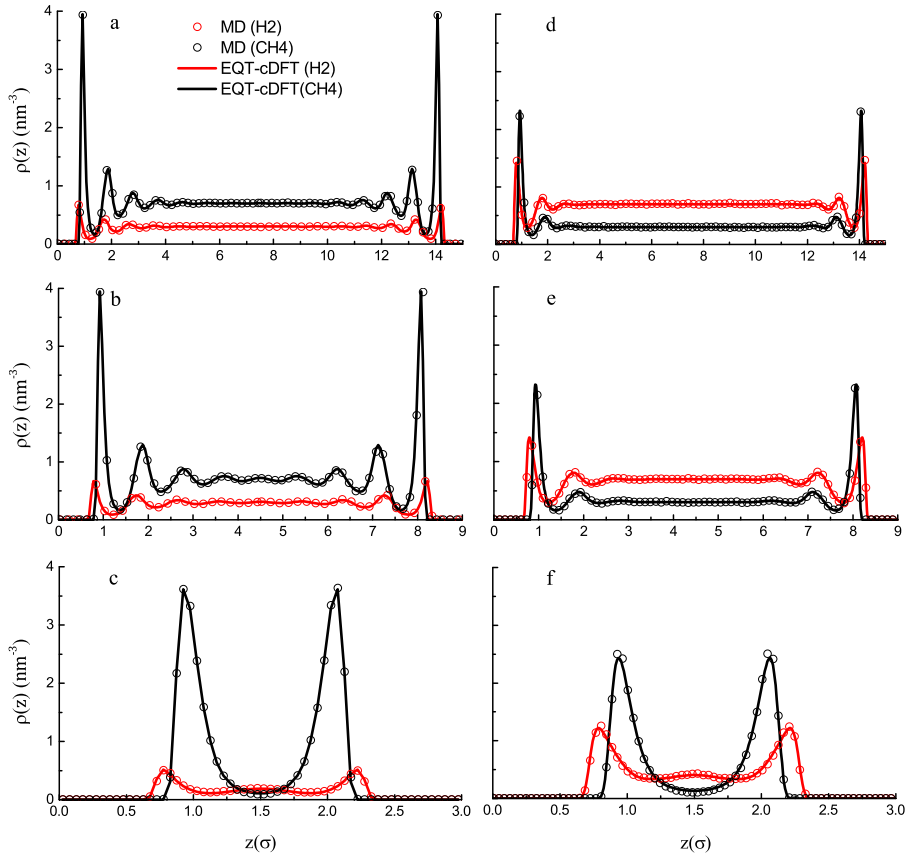

FIG. 2. Comparison of density profiles of methane and hydrogen from EQT-cDFT and MD simulations for different channel widths in equilibrium with methane-rich ((a)-(c)) and hydrogen-rich ((d)-(f)) bulk mixtures.

and hydrogen density profiles are normalized by the density of the bulk mixture which is 17.73 nm^{-3}. Thus, the bulk values for large channels (see Figs. 2(a) and 2(d)) reflect the molar composition of each species in the bulk mixture. Apart from the middle of the channel, both methane and hydrogen molecules arrange in layers due to the interplay of wall-fluid and fluid-fluid interactions. As the channels become narrower, the wall-fluid potential of two interfaces starts to overlap and the bulk-like region disappears. Comparing Figs. 2(a)–2(f), the density profiles associated with $x_m = 0.7$ exhibit an enhanced layering in comparison with $x_m = 0.3$ density profiles. In addition, it can be seen that, irrespective of the bulk molar composition, the graphene wall preferably selects methane over the hydrogen molecules.

Fig. 3 shows the variation of the average density of each species with the channel width and the bulk composition. For channels in equilibrium with the methane-rich bulk mixture, both methane and hydrogen average densities monotonically decrease (slight undulations) until $H = 6\sigma_m$. As the channel width further decreases, we observe noticeable undulations in the average densities versus H. These oscillations in ρ_{avg} for smaller channels follow the formation of adsorbed layers with increasing H. A similar trend has been observed for hydrogen average density for channels in equilibrium with the hydrogen-rich bulk mixture. However, the onset of undulations has been observed for $4\sigma_m$ channel width. Moreover, unlike the $x_m = 0.7$ case, the methane average density in the channel is higher than its bulk density and grows monotonically until $H = 4\sigma_m$. For the $15\sigma_m$ channel, the hydrogen average density is higher than that of methane. As the channel width gets smaller, hydrogen molecules get depleted from the channel and are replaced by methane molecules. This trend continues, until the number of methane molecules surpasses the hydrogen molecules in the channel of $3.25\sigma_m$ width. Further decrease in the channel width results in the adsorption of more methane molecules in comparison to hydrogen, despite the fact that the bulk mixture is rich in hydrogen content. Therefore, we can clearly see how graphene is selective towards methane. In fact, the origin of this behavior is rooted in the higher interaction energy between carbon-methane compared to carbon-hydrogen.

Fig. 4 shows the variation of the lateral pressure tensor profiles in the channels corresponding to the methane and hydrogen-rich bulk mixtures. It can be seen that the EQT-cDFT predictions are in good agreement with the MD simulations.

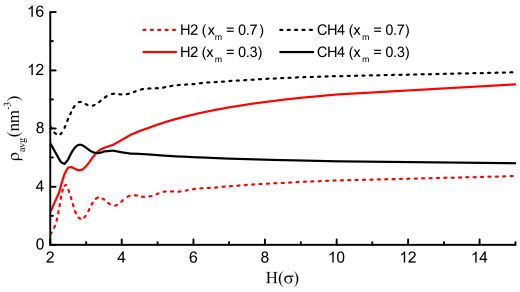

FIG. 3. EQT-cDFT predictions for average densities of methane and hydrogen molecules as a function of channel width.

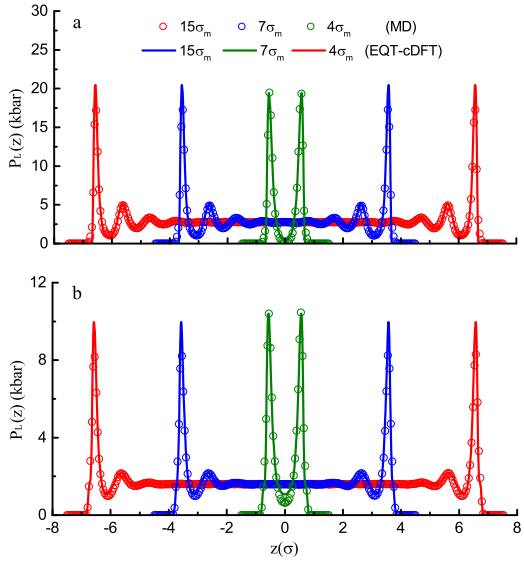

FIG. 4. Comparison of lateral pressure profiles of methane-rich mixture (a) and hydrogen-rich mixture (b) from EQT-cDFT and MD simulations for various channel widths.

As it is evident from Eq. (20), due to the layering in the density profiles, an oscillatory behavior is also observed in the lateral pressure profiles. We observe that in confinement, the lateral pressure is significantly enhanced compared to its bulk value. This effect is more pronounced in the vicinity of the walls, where the value of the pressure is approximately 5 times higher than the bulk value for the $15\sigma_m$ channel (see Fig. 4(b)). Such high values of pressure can enhance chemical reactions and give rise to high pressure solid phases in nanoconfinements.[4,82–85]

From Figs. 2 and 4, we observe that the high lateral pressure regions correspond to the locations where the methane density profile exhibits peaks. Even though hydrogen molecules also contribute to the pressure, due to their smaller diameter and interaction energy compared to methane, the lateral pressure profiles follow closely the methane density profiles, irrespective of the bulk mixture composition. This fact is more evident as the channel width gets smaller. The higher adsorption affinity of methane in the narrower channels[31] makes it the dominant contributor to lateral pressure in these channels.

By comparing Figs. 4(a) and 4(b), we find that the channels in equilibrium with the methane-rich bulk mixture exhibit higher pressure. In addition, by looking at the $15\sigma_m$ channels, it is clear that by increasing the methane content of the bulk, the oscillations in the lateral pressure profile become more pronounced and decay slower than the hydrogen-rich bulk mixture to the bulk value. The origin of this behavior lies in the tendency of graphene for attracting methane molecules over hydrogen, and the ordering enhancement caused by the methane molecules (compare Figs. 2(b) and 2(e)) in confinement.

In Fig. 5, we show the variation of the normal pressure, solvation force, and surface tension as a function of the channel width for both methane and hydrogen-rich bulk mixtures. We observe that the theoretical predictions by the EQT-cDFT approach compare well with MD simulations. As mentioned

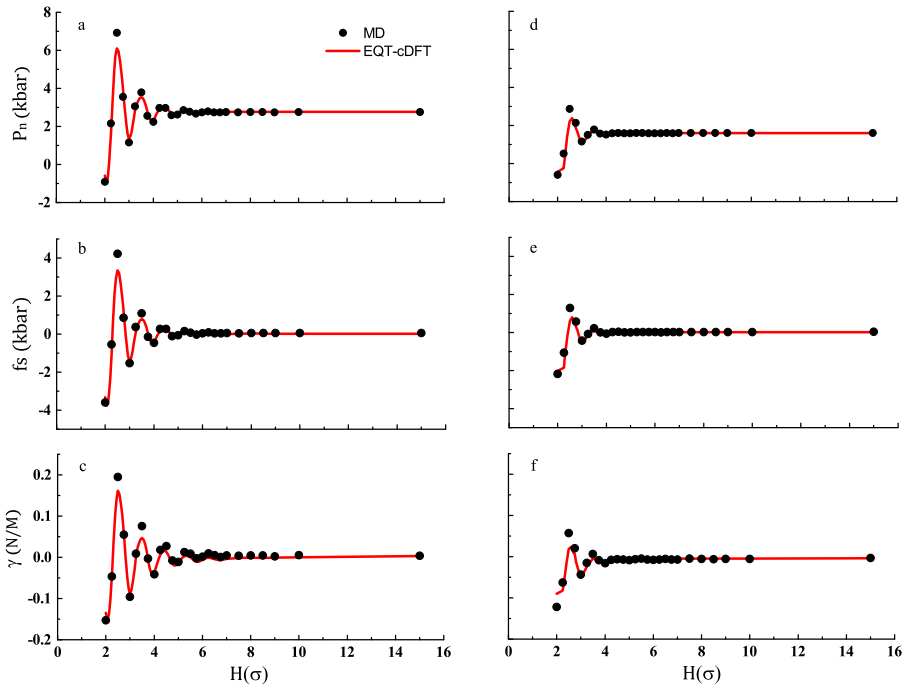

FIG. 5. Variation of normal pressure (P_n), solvation force (f_s), and surface tension (γ) with the channel width corresponding to the methane-rich ((a)-(c)) and hydrogen-rich ((d)-(f)) bulk mixture compositions.

in Sec. II, due to the mechanical equilibrium, for a slit channel, normal pressure is constant across the channel width (i.e., independent of z). However, it shows an oscillatory behavior as a function of the channel width. These oscillations are well-known and relate to the number of adsorbate layers, the interlayer spacing,[86] and the behavior of the average density,[82,87] which depends on the channel width. As a corollary, the solvation force and surface tension also exhibit an oscillatory behavior with decaying amplitude as the channel width gets larger. For larger channels, the wall effects become weaker and hence P_n converges to the bulk value, and f_s and γ approach zero.

To investigate the effect of mixture composition and its constituents, we focus our attention on Figs. 5(a)–5(f). It can be seen that for $x_m = 0.7$ bulk composition, the maximum value of the normal pressure is about 3 times higher than that of channels in equilibrium with $x_m = 0.3$ bulk mixture. Moreover, we observe that the oscillations in f_s (Fig. 5(e)) disappear at $4.25\sigma_m$ for $x_m = 0.3$, whereas for the channels in equilibrium with the methane-rich bulk mixture, the oscillations persist until $6.6\sigma_m$. Again, this confirms the observations that for the channels in equilibrium with the methane-rich mixture, the extent of oscillatory behavior observed in thermodynamic properties is larger compared to the bulk composition of $x_m = 0.3$.

V. CONCLUSIONS

In the present study, we showed that using the EQT-based potentials, we can construct an expression for the excess free energy functional in the cDFT framework to obtain various thermodynamic properties, such as density, local pressure tensor, solvation force, and surface tension. We demonstrated the EQT-cDFT approach for a binary mixture of methane and hydrogen molecules confined in slit nanochannels of various widths and two different bulk compositions. We found that our theoretical predictions compare well with the MD simulations, showing that the EQT-cDFT is a promising approach to obtain thermodynamic properties of confined fluid mixtures.

ACKNOWLEDGMENTS

This work was supported by NSF under Grant Nos. 1264282, 1420882, 1506619, and 1545907 and AFOSR under Grant No. FA9550-12-1-0464. The authors acknowledge the use of the Taub cluster provided by the Computational Science and Engineering Program at the University of Illinois.

[1] C. Alba-Simionesco, B. Coasne, G. Dosseh, G. Dudziak, K. Gubbins, R. Radhakrishnan, and M. Sliwinska-Bartkowiak, J. Phys.: Condens. Matter **18**, R15 (2006).
[2] G. A. Mansoori, *Principles of Nanotechnology: Molecular-Based Study of Condensed Matter in Small Systems* (World Scientific, 2005).
[3] C. A. Miller and P. Neogi, *Interfacial Phenomena: Equilibrium and Dynamic Effects* (CRC Press, 2007), Vol. 139.
[4] Y. Long, J. C. Palmer, B. Coasne, M. Śliwinska Bartkowiak, and K. E. Gubbins, Phys. Chem. Chem. Phys. **13**, 17163 (2011).
[5] G. A. Mansoori and S. A. Rice, Adv. Chem. Phys. **156**, 197 (2014).
[6] S. Han, M. Choi, P. Kumar, and H. E. Stanley, Nat. Phys. **6**, 685 (2010).
[7] A. Barati Farimani and N. R. Aluru, J. Phys. Chem. C **120**, 23763 (2016).
[8] A. Barati Farimani and N. Aluru, J. Phys. Chem. B **115**, 12145 (2011).
[9] X. Qin, Q. Yuan, Y. Zhao, S. Xie, and Z. Liu, Nano Lett. **11**, 2173 (2011).
[10] J. Wu, AIChE J. **52**, 1169 (2006).
[11] M. E. Suk, A. V. Raghunathan, and N. R. Aluru, Appl. Phys. Lett. **92**, 133120 (2008).
[12] J. Han, J. Fu, and R. B. Schoch, Lab Chip **8**, 23 (2007).
[13] K. P. Lee, T. C. Arnot, and D. Mattia, J. Membr. Sci. **370**, 1 (2011).
[14] N. Hilal, H. Al-Zoubi, N. A. Darwish, A. W. Mohammad, and M. Abu Arabi, Desalination **170**, 281 (2004).
[15] C. Smith, Nature **446**, 219 (2007).
[16] A. F. Azarbayjani, A. Jouyban, and S. Y. Chan, J. Pharm. Pharm. Sci. **12**, 218 (2009).
[17] B. A. Suleimanov, F. S. Ismailov, and E. F. Veliyev, J. Pet. Sci. Eng. **78**, 431 (2011).
[18] D. A. Z. Wever, F. Picchioni, and A. A. Broekhuis, Prog. Polym. Sci. **36**, 1558 (2011).
[19] K. Urita, Y. Shiga, T. Fujimori, T. Iiyama, Y. Hattori, H. Kanoh, T. Ohba, H. Tanaka, M. Yudasaka, S. Iijima, I. Moriguchi, F. Okino, M. Endo, and K. Kaneko, J. Am. Chem. Soc. **133**, 10344 (2011).

[20]P. T. Cummings, H. Docherty, C. R. Iacovella, and J. K. Singh, AIChE J. **56**, 842 (2010).
[21]L. D. Gelb, K. Gubbins, R. Radhakrishnan, and M. Sliwinska-Bartkowiak, Rep. Prog. Phys. **62**, 1573 (1999).
[22]M. P. Allen and D. J. Tildesley, *Computer Simulation of Liquids* (Oxford University Press, 1989).
[23]D. Frenkel and B. Smit, *Understanding Molecular Simulation: From Algorithms to Applications* (Academic Press, 2001).
[24]K. E. Gubbins, Y.-C. Liu, J. D. Moore, and J. C. Palmer, Phys. Chem. Chem. Phys. **13**, 58 (2011).
[25]R. Qiao and N. R. Aluru, J. Chem. Phys. **118**, 4692 (2003).
[26]A. V. Raghunathan, J. H. Park, and N. R. Aluru, J. Chem. Phys. **127**, 174701 (2007).
[27]T. Sanghi and N. R. Aluru, J. Chem. Phys. **132**, 044703 (2010).
[28]T. Sanghi and N. R. Aluru, J. Chem. Phys. **136**, 024102 (2012).
[29]S. Y. Mashayak and N. R. Aluru, J. Chem. Theory Comput. **8**, 1828 (2012).
[30]S. Y. Mashayak and N. R. Aluru, J. Chem. Phys. **137**, 214707 (2012).
[31]M. Motevaselian, S. Mashayak, and N. Aluru, J. Chem. Phys. **143**, 124106 (2015).
[32]S. Mashayak, M. Motevaselian, and N. Aluru, J. Chem. Phys. **142**, 244116 (2015).
[33]C. Ebner, W. F. Saam, and D. Stroud, Phys. Rev. A **14**, 2264 (1976).
[34]N. D. Mermin, Phys. Rev. **137**, A1441 (1965).
[35]J.-P. Hansen and I. R. McDonald, in *Theory of Simple Liquids*, 4th ed., edited by J.-P. Hansen and I. R. McDonald (Academic Press, Oxford, 2013), pp. 203–264.
[36]R. Evans, Lectures at 3rd Warsaw School of Statistical Physics, Kazimierz Dolny, 27, 2009.
[37]F.-Q. You, Y.-X. Yu, and G.-H. Gao, J. Phys. Chem. B **109**, 3512 (2005).
[38]Y.-X. Yu, F.-Q. You, Y. Tang, G.-H. Gao, and Y.-G. Li, J. Phys. Chem. B **110**, 334 (2006).
[39]P. Tarazona, Phys. Rev. A **31**, 2672 (1985).
[40]F. van Swol and J. Henderson, Phys. Rev. A **43**, 2932 (1991).
[41]B. Peng and Y.-X. Yu, J. Phys. Chem. B **112**, 15407 (2008).
[42]Y. Rosenfeld, J. Chem. Phys. **98**, 8126 (1993).
[43]Y. Rosenfeld, M. Schmidt, H. Lwen, and P. Tarazona, Phys. Rev. E **55**, 4245 (1997).
[44]Y. Tang and J. Wu, J. Chem. Phys. **119**, 7388 (2003).
[45]N. Choudhury and S. K. Ghosh, J. Phys. Chem. B **107**, 7155 (2003).
[46]Y.-X. Yu, G.-H. Gao, and X.-L. Wang, J. Phys. Chem. B **110**, 14418 (2006).
[47]J. Puibasset, E. Kierlik, and G. Tarjus, J. Chem. Phys. **141**, 044716 (2014).
[48]R. Evans, M. Oettel, R. Roth, G. Kahl, and H. Hansen-Goos, J. Phys.: Condens. Matter **28**, 240401 (2016).
[49]F. Lado, Mol. Phys. **107**, 301 (2009).
[50]E. Kierlik and M. L. Rosinberg, Phys. Rev. A **44**, 5025 (1991).
[51]M. Sliwinska-Bartkowiak, R. Sikorski, S. Sowers, L. Gelb, and K. Gubbins, Fluid Phase Equilib. **136**, 93 (1997).
[52]S. Toxvaerd, J. Chem. Phys. **64**, 2863 (1976).
[53]J. C. Barrett, J. Chem. Phys. **124**, 144705 (2006).
[54]G. J. Gloor, G. Jackson, F. Blas, E. M. Del Rio, and E. De Miguel, J. Phys. Chem. C **111**, 15513 (2007).
[55]P. Lurie-Gregg, J. B. Schulte, and D. Roundy, Phys. Rev. E **90**, 042130 (2014).
[56]J. Lebowitz, Phys. Rev. **133**, A895 (1964).
[57]P. Leonard, D. Henderson, and J. Barker, Mol. Phys. **21**, 107 (1971).
[58]J. A. Barker and D. Henderson, J. Chem. Phys. **47**, 4714 (1967).
[59]H. Löwen, J. Phys.: Condens. Matter **14**, 11897 (2002).
[60]S. Zhao, H. Liu, R. Ramirez, and D. Borgis, J. Chem. Phys. **139**, 034503 (2013).
[61]R. Roth, R. Evans, A. Lang, and G. Kahl, J. Phys.: Condens. Matter **14**, 12063 (2002).
[62]R. Roth, J. Phys.: Condens. Matter **22**, 063102 (2010).
[63]Y.-X. Yu and J. Wu, J. Chem. Phys. **117**, 2368 (2002).
[64]Y.-X. Yu, J. Wu, Y.-X. Xin, and G.-H. Gao, J. Chem. Phys. **121**, 1535 (2004).
[65]Y.-X. Yu, J. Chem. Phys. **131**, 024704 (2009).
[66]L. F. Vega and G. Jackson, Fluid Phase Equilib. **306**, 1 (2011).
[67]J. Hughes, E. J. Krebs, and D. Roundy, J. Chem. Phys. **138**, 024509 (2013).
[68]K. Gong, B. D. Marshall, and W. G. Chapman, J. Chem. Phys. **139**, 094904 (2013).
[69]E. J. Krebs, J. B. Schulte, and D. Roundy, J. Chem. Phys. **140**, 124507 (2014).
[70]O. Berger, O. Edholm, and F. Jähnig, Biophys. J. **72**, 2002 (1997).
[71]E. de Miguel and G. Jackson, J. Chem. Phys. **125**, 164109 (2006).
[72]E. Kierlik, Y. Fan, P. Monson, and M. Rosinberg, J. Chem. Phys. **102**, 3712 (1995).
[73]J. Henderson and F. van Swol, Mol. Phys. **51**, 991 (1984).
[74]F. van Swol and J. R. Henderson, Phys. Rev. A **40**, 2567 (1989).
[75]M. P. Allen, Chem. Phys. Lett. **331**, 513 (2000).
[76]J. G. Kirkwood and F. P. Buff, J. Chem. Phys. **17**, 338 (1949).
[77]S. H. Lee, J. C. Rasaiah, and J. Hubbard, J. Chem. Phys. **86**, 2383 (1987).
[78]S. K. Bhatia and D. Nicholson, Phys. Rev. Lett. **100**, 236103 (2008).
[79]S. Pronk, S. Pll, R. Schulz, P. Larsson, P. Bjelkmar, R. Apostolov, M. R. Shirts, J. C. Smith, P. M. Kasson, D. van der Spoel, B. Hess, and E. Lindahl, Bioinformatics **29**, 845 (2013).
[80]J. M. Vanegas, A. Torres-Sánchez, and M. Arroyo, J. Chem. Theory Comput. **10**, 691 (2014).
[81]P. Kumar, S. V. Buldyrev, F. W. Starr, N. Giovambattista, and H. E. Stanley, Phys. Rev. E **72**, 051503 (2005).
[82]J. Klein and E. Kumacheva, Science **269**, 816 (1995).
[83]M. Heuberger, M. Zch, and N. D. Spencer, Science **292**, 905 (2001).
[84]Y. Long, J. C. Palmer, B. Coasne, M. Śliwinska Bartkowiak, G. Jackson, E. A. Müller, and K. E. Gubbins, J. Chem. Phys. **139**, 144701 (2013).
[85]K. E. Gubbins, Y. Long, and M. Śliwinska-Bartkowiak, J. Chem. Thermodyn. **74**, 169 (2014).
[86]B. Coasne, Y. Long, and K. Gubbins, Mol. Simul. **40**, 721 (2014).
[87]H. Eslami and N. Mehdipour, J. Chem. Phys. **137**, 144702 (2012).